

# Regression Analysis for Transport Electron Scattering Caused by Structural Defects in InSb Quantum Wells: Application of Matthiessen's Formula

Tetsuya D. Mishima\* and Michael B. Santos

Homer L. Dodge Department of Physics and Astronomy, and Center for Semiconductor Physics in Nanostructures, University of Oklahoma, Norman, OK 73019, U.S.A.

Received November 29, 2011; accepted February 23, 2012; published online June 20, 2012

The graphical representation and numerical interpretation of the results obtained by a regression analysis for Matthiessen's formula have been investigated for the electron scattering due to micro-twins (MTs) and threading dislocations (TDs) in InSb quantum wells (QWs) at room temperature. By plotting the reciprocal of the total mobility vs the summation of the linear terms due to MTs and TDs, a two-dimensional graphical representation that clearly exhibits the "goodness of fit" of the regression analysis was depicted. The usefulness of numerical indexes, "effective defect density" and "equivalent defect scattering", was discussed: "effective defect density" made it possible to evaluate the electron scattering in InSb QWs by using one type of structural defects, either MTs or TDs. "Equivalent defect scattering" enables one to intuitively grasp the difference in magnitude of electron scattering between MTs and TDs in InSb QWs. © 2012 The Japan Society of Applied Physics

## 1. Introduction

Among all the binary III–V semiconductors, InSb has the highest electron mobility [ $77,000 \text{ cm}^2/(\text{V}\cdot\text{s})$ ] and the narrowest band-gap (0.18 eV) at room temperature.<sup>1)</sup> InSb is often used as a form of a quantum well (QW) structure, in order to fully exploit the remarkable properties of InSb. The actual performance of InSb-QW-based devices, however, is significantly limited by structural defects. Transmission electron microscopy (TEM) analyses showed that micro-twins (MTs) and threading dislocations (TDs) are dominant structural defects in InSb QWs grown on GaAs(001) substrates,<sup>2–4)</sup> which are common choices of substrates for InSb-QW-based devices.<sup>5–11)</sup> These defects degrade the total electron mobilities in InSb QWs.<sup>4,12,13)</sup>

Based on regression analyses for Matthiessen's law, recently we have reported quantitative studies for electron scattering due to both TD and MT defects in InSb QWs,<sup>12,13)</sup> although the effect of these defects on electron transport in InSb epilayers<sup>14–19)</sup> and non-InSb two-dimensional (2D) systems<sup>20–25)</sup> which include QW structures has long been investigated. By using the results of a regression analysis, the energy barrier height and reflection coefficient were deduced to be  $\sim 0.087 \text{ eV}$  and  $\sim 0.33$ , respectively, for the room-temperature electron scattering due to a MT in 20-nm-thick InSb QWs.<sup>13)</sup> Under the *assumption* that the electron scattering due to a TD is fully attributed to its electric field, the electric charge of a TD is  $1.7 \times 10^{-10} \text{ C/m}$  along the [001] direction which is perpendicular to the InSb QWs.<sup>13)</sup> The mobility limits due to the TDs and MTs estimated based on a regression analysis were plotted by using their "percentage impacts", which clearly show their individual contributions upon the total electron mobility in the InSb QWs.<sup>12)</sup>

In this paper, we expand our previous discussion<sup>12,13)</sup> about a regression analysis for the electron scattering due to MTs and TDs in InSb QWs at room temperature. This time we focus on the graphical representation and the numerical interpretation of the direct results (defect coefficients:  $A_{\text{defect}}$ ) obtained by a regression analysis.

## 2. Experimental Procedure

Nine of Si-remotely-doped InSb QW structures grown on GaAs(001) substrates by molecular beam epitaxy were used for this study. The InSb QW layers which were sandwiched with  $\text{Al}_{0.2}\text{In}_{0.8}\text{Sb}$  barrier layers have a thickness of 20 nm. These InSb QWs, however, have different densities of MT and TD defects, which were intentionally varied by using GaAs(001) substrates with different surface miscut ( $0 \pm 0.5$  or  $2 \pm 0.5^\circ$ ) and AlInSb-based buffer layers with different structure.<sup>3,4)</sup> Transmission electron microscopy was employed to measure MT and TD densities in InSb QWs.<sup>2–4,26,27)</sup> The sheet electron densities of the nine InSb QW structures, which were deduced from the van der Pauw and Hall effect measurements,<sup>28)</sup> range from  $4.1 \times 10^{11}$  to  $5.7 \times 10^{11} / \text{cm}^2$ . The average sheet electron density is  $4.8 \times 10^{11} / \text{cm}^2$  with a standard deviation of  $0.5 \times 10^{11} / \text{cm}^2$ . Part of the deviation may be derived from the variation in defect density among the InSb QWs.<sup>15,18)</sup> A regression analysis was performed with a statistical software package R.<sup>29)</sup> Detailed descriptions of InSb QW structures and experimental conditions can be found elsewhere.<sup>4,13)</sup>

## 3. Matthiessen's Formula and Its Linear Regression Analysis

According to Matthiessen's rule, the reciprocal of the total electron mobility  $\mu_{\text{total}}$  in an InSb QW that contains MT and TD defects is expressed as

$$\frac{1}{\mu_{\text{total}}} = \frac{1}{\mu_{\text{MT}}} + \frac{1}{\mu_{\text{TD}}} + \frac{1}{\mu_{\text{others}}}, \quad (1)$$

where  $\mu_{\text{MT}}$ ,  $\mu_{\text{TD}}$ , and  $\mu_{\text{others}}$  are the mobility limits due to MTs, TDs, and all the other scattering factors, respectively.<sup>12,13)</sup> In general, the reciprocal of the mobility limit  $\mu_{\text{defect}}$  due to a type of structural defect is equal to the product of the defect density and a constant. When this relation is applicable to MTs and TDs in InSb QWs, eq. (1) can be transformed into

$$\frac{1}{\mu_{\text{total}}} = A_{\text{MT}} D_{\text{MT}} + A_{\text{TD}} D_{\text{TD}} + \frac{1}{\mu_{\text{others}}}, \quad (2)$$

where  $D_{\text{MT}}$  and  $D_{\text{TD}}$  are the densities of MTs and TDs, respectively, and  $A_{\text{MT}}$  and  $A_{\text{TD}}$  are corresponding coeffi-

\*E-mail address: mishima@ou.edu

cients. Equation (2) can be regarded as one of the linear equations that have a general form of

$$y = a_1x_1 + a_2x_2 + b. \quad (3)$$

This indicates that the values of  $A_{MT}$ ,  $A_{TD}$ , and  $1/\mu_{\text{others}}$  can be determined statistically by using a multiple linear regression,<sup>29)</sup> when the experimental values of  $1/\mu_{\text{total}}$ ,  $D_{MT}$ , and  $D_{TD}$  are available.

We obtained nine of  $(1/\mu_{\text{total}}, D_{MT}, D_{TD})$  data sets from InSb QWs whose average sheet electron density is  $4.8 \times 10^{11}/\text{cm}^2$ . For these experimental data, the ‘‘sample correlation coefficient’’ between  $D_{MT}$ , and  $D_{TD}$  was calculated to be 0.42, which should be low enough to treat  $D_{MT}$ , and  $D_{TD}$  as mutually independent variables in a regression analysis.<sup>13)</sup> By using eq. (2) with the experimental data, we performed a regression analysis in the same fashion as can be seen elsewhere.<sup>12,13)</sup> The coefficient of determination  $R^2$  resulted in 0.9791. The regression analysis showed that  $A_{MT}$ ,  $A_{TD}$ , and  $1/\mu_{\text{others}}$  are  $7.9 \times 10^{-10} \text{ V}\cdot\text{s}/\text{cm}$ ,  $5.9 \times 10^{-15} \text{ V}\cdot\text{s}$ , and  $1.7 \times 10^{-5} \text{ V}\cdot\text{s}/\text{cm}^2$ , respectively, at room temperature for the InSb QWs examined in this study. It is expected that  $A_{MT}$ ,  $A_{TD}$ , and  $1/\mu_{\text{others}}$  can take different values depending on the design and quality of InSb QWs,<sup>30)</sup> as well as their average sheet electron density.<sup>23,30)</sup>

#### 4. Three-Dimensional Representation of Regression Analysis

Figure 1(a) shows a three-dimensional (3D) representation of the results of the above-mentioned regression analysis, which was performed with eq. (2) for the case of InSb QWs at room temperature. The experimental data used for the analysis were plotted with gray and black spheres in the Cartesian coordinate system with  $D_{MT}$ ,  $D_{TD}$ , and  $1/\mu_{\text{total}}$  axes. Equation (2) represents a plane in the  $D_{MT} - D_{TD} - 1/\mu_{\text{total}}$  coordinate system, since eq. (3), which has a similar form to eq. (2), can be regarded as a general equation for a geometric ‘‘plane’’ in a 3D space. With the determined  $A_{MT}$ ,  $A_{TD}$ , and  $1/\mu_{\text{others}}$  values by the regression analysis, eq. (2) actually shows a *regression plane* that represents a linear nature of the experimental data. In Fig. 1(a), all the experimental data (gray and black spheres) are located close to the regression plane which was denoted with a (multi-colored) rectangular mesh grid. By using a stereographic projection technique, one may be able to recognize the geometric relations between the experimental data and the regression plane more clearly. Figure 1(b) is the stereo pair to Fig. 1(a). By looking at Figs. 1(a) and 1(b) with left and right eyes, respectively, one can perceive the graph in a virtual 3D space: the experimental data depicted with gray and black spheres should appear slightly above and below the regression plane, respectively.

Although the stereo graphs of Figs. 1(a) and 1(b) may be useful to grasp the results of the regression analysis intuitively, they are not really suitable to quantitatively show the deviation in  $1/\mu_{\text{total}}$  between the individual experimental data and the regression plane, which is one of the most important values that need to be checked after the regression analysis. If the deviations are large, they might be visualized with ‘‘drop lines’’ that are drawn from the data points to the regression plane.<sup>29)</sup> In the case of

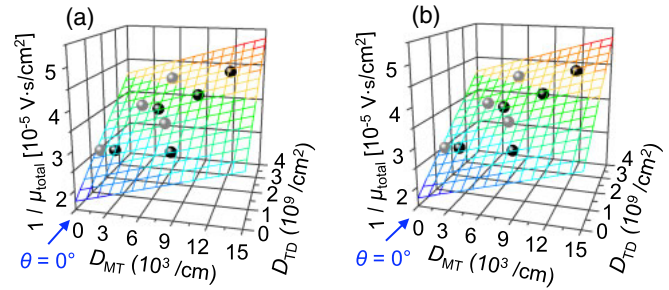


**Fig. 1.** (Color online) Pair of stereographic 3D graphs for  $1/\mu_{\text{total}}$ ,  $D_{MT}$ , and  $D_{TD}$  measured from nine InSb QW structures. In both (a) and (b), regression planes are represented by (multi-colored) mesh grids. Gray and black spheres correspond to data points located above and below the regression planes, respectively. The  $D_{TD}$  axes are shown by the arrows, with respect to which the rotation angle  $\theta$  about the  $1/\mu_{\text{total}}$  axis is measured [see also Fig. 2(b)]. By looking at (a) and (b) with left and right eyes, respectively, one can recognize the graph in a virtual 3D space with the feeling of pseudo perspective.

MT and TD scattering in InSb QWs, however, such drop lines are all too short to exhibit differences apparently in Figs. 1(a) and 1(b), since the experimental data are closely located around the regression plane with a good  $R^2$  value of 0.9791.

#### 5. Two-Dimensional Representation of Regression Analysis

When the 3D graphs shown in Figs. 1(a) and 1(b) are projected onto a 2D plane from a certain direction, we can clearly perceive the deviations between the experimental data and the regression plane. Figures 2(a)–2(e) show the 3D graphs which are viewed from different directions. The viewing direction for Fig. 2(a) is *parallel* to the  $D_{TD}$  axis [see also Figs. 1(a) and 1(b) for the position of the  $D_{TD}$  axis], although objects located in the off-center area (including the  $D_{TD}$  axis itself) appear to fan out. This is because Fig. 2(a) was drawn with a perspective technique. The rotation angle  $\theta$  of the 3D graph around the  $1/\mu_{\text{total}}$  axis [see Fig. 2(b)] is zero ( $\theta = 0^\circ$ ) for Fig. 2(a). Figures 2(b)–2(e) depict the 3D graphs viewed with rotation angles of  $\theta = 30, 63.4, 80,$  and  $90^\circ$ , respectively. In Fig. 2(c), the regression plane is seen as a regression *line* when the rotation angle is  $\theta = 63.4^\circ$  (see Appendix B for the reason). Since the  $1/\mu_{\text{total}}$  axis coincides with the vertical direction of this figure, the vertical distances between the experimental data and the regression line should be *roughly* proportional to the corresponding deviations in  $1/\mu_{\text{total}}$ . Due to the fan-out effect of 3D perspective, however, the deviations are not accurately displayed in Fig. 2(c). In the off-center area, the experimental plots shallowly (deeply) located than the  $1/\mu_{\text{total}}$  axis in the 3D space yield a slightly larger (smaller) deviation in Fig. 2(c) than their actual values. Similar artifacts also take place for the lateral positions of the experimental data.

Plotting  $1/\mu_{\text{total}}$  values with respect to  $(A_{MT}D_{MT} + A_{TD}D_{TD})$  directly onto a 2D graph, as shown in Fig. 3(a), is one way to solve the inaccuracy issue of the 2D projection shown in Fig. 2(c). [Detailed explanations about Fig. 3(a) can be found in Appendix A.] This means that one can obtain accurate visual representations of the ‘‘goodness of

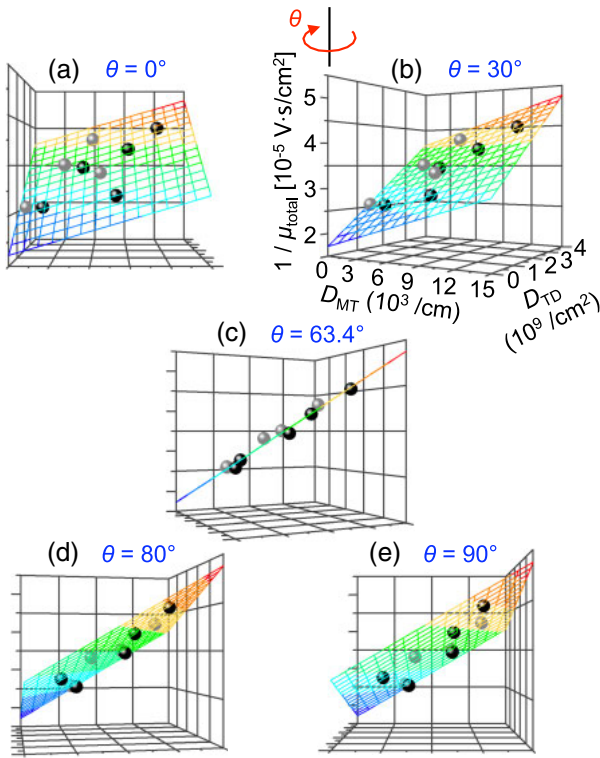


**Fig. 2.** (Color online) Different views of the 3D graphs shown in Figs. 1(a) and 1(b). The rotation angles  $\theta$  for (a), (b), (c), (d), and (e) about the  $1/\mu_{\text{total}}$  axis are 0, 30, 63.4, 80, and 90°, respectively. The labels of axes are shown only in (b), for simplicity. The regression plane is seen as a line in (c).

fit”, by dealing with the two linear terms in the original regression equation of eq. (2) together. Although the arrangements of the experimental data in Figs. 2(c) and 3(a) resemble each other, the accurate deviations between the experimental data and the regression line are only seen in Fig. 3(a).

The 2D graphical representation discussed above can also be applicable to the regression analyses for general linear equations that have more than two linear terms. A simple mathematical induction can be used for the proof.

## 6. Numerical Indexes for Defect Scattering

### 6.1 Effective defect density

In the previous section, we showed that a 2D graphical expression for eq. (2) can be drawn by plotting  $[(A_{\text{MT}}D_{\text{MT}} + A_{\text{TD}}D_{\text{TD}}), 1/\mu_{\text{total}}]$ . More generally, however, when  $1/\mu_{\text{total}}$  values are plotted with respect to  $k(A_{\text{MT}}D_{\text{MT}} + A_{\text{TD}}D_{\text{TD}})$  where  $k$  is a non-zero constant, the deviations between the experimental  $1/\mu_{\text{total}}$  values and the regression result can also be shown correctly on a 2D graph. When  $k$  value is  $k = 1/A_{\text{MT}}$ , the horizontal axis of a 2D graph becomes  $(A_{\text{MT}}D_{\text{MT}} + A_{\text{TD}}D_{\text{TD}})/A_{\text{MT}} = D_{\text{MT}} + (A_{\text{TD}}/A_{\text{MT}})D_{\text{TD}}$ . Figure 3(b) shows such a graph, which has a similar appearance to Fig. 3(a) as expected. Equation (2) can be transformed into

$$\frac{1}{\mu_{\text{total}}} = A_{\text{MT}} \left( D_{\text{MT}} + \frac{A_{\text{TD}}}{A_{\text{MT}}} D_{\text{TD}} \right) + \frac{1}{\mu_{\text{others}}}. \quad (4)$$

This shows that the slope and intercept of the regression line in Fig. 3(b) correspond to  $A_{\text{MT}}$  and  $1/\mu_{\text{others}}$  values,

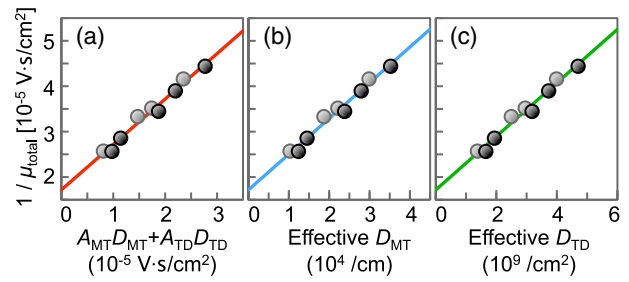


**Fig. 3.** (Color online) 2D representations of a multiple linear regression analysis for  $1/\mu_{\text{total}}$ ,  $D_{\text{MT}}$ , and  $D_{\text{TD}}$  measured from InSb QWs at room temperature.  $1/\mu_{\text{total}}$  are plotted as functions of (a)  $A_{\text{MT}}D_{\text{MT}} + A_{\text{TD}}D_{\text{TD}}$ , (b) effective  $D_{\text{MT}} [= D_{\text{MT}} + (A_{\text{TD}}/A_{\text{MT}})D_{\text{TD}}]$  and (c) effective  $D_{\text{TD}} [= (A_{\text{MT}}/A_{\text{TD}})D_{\text{MT}} + D_{\text{TD}}]$ . The experimental data are seen as gray and black spheres, whose color schemes are the same as in Figs. 1 and 2. In (a)–(c), regression lines are shown in different colors.

respectively. In eq. (4),  $D_{\text{MT}} + (A_{\text{TD}}/A_{\text{MT}})D_{\text{TD}}$  has a coefficient of  $A_{\text{MT}}$ , which was originally defined as a coefficient for  $D_{\text{MT}}$ . This indicates that  $D_{\text{MT}} + (A_{\text{TD}}/A_{\text{MT}})D_{\text{TD}}$  has the same unit (say, /cm) as  $D_{\text{MT}}$  does.  $D_{\text{MT}} + (A_{\text{TD}}/A_{\text{MT}})D_{\text{TD}}$  can be interpreted as an “effective MT density”: the density of TDs,  $D_{\text{TD}}$ , appears to be converted to an equivalent MT density in terms of electron scattering, by being multiplied by a conversion factor of  $(A_{\text{TD}}/A_{\text{MT}})$ . Therefore, in the expression of  $D_{\text{MT}} + (A_{\text{TD}}/A_{\text{MT}})D_{\text{TD}}$ , the effects of both MTs and TDs on carrier scattering are fully expressed in the form of MT densities.

When we choose another  $k$  value of  $k = 1/A_{\text{TD}}$ ,  $k(A_{\text{MT}}D_{\text{MT}} + A_{\text{TD}}D_{\text{TD}})$  becomes  $(A_{\text{MT}}/A_{\text{TD}})D_{\text{MT}} + D_{\text{TD}}$ . A 2D representation similar to those shown in Figs. 3(a) and 3(b) can be obtained by using  $(A_{\text{MT}}/A_{\text{TD}})D_{\text{MT}} + D_{\text{TD}}$  as horizontal values, as shown in Fig. 3(c). In this case, the slope and intercept of the regression line correspond to  $A_{\text{TD}}$  and  $1/\mu_{\text{others}}$  values, respectively, since eq. (2) can be transformed into

$$\frac{1}{\mu_{\text{total}}} = A_{\text{TD}} \left( \frac{A_{\text{MT}}}{A_{\text{TD}}} D_{\text{MT}} + D_{\text{TD}} \right) + \frac{1}{\mu_{\text{others}}}. \quad (5)$$

$(A_{\text{MT}}/A_{\text{TD}})D_{\text{MT}} + D_{\text{TD}}$  can be treated as an effective TD density, due to a similar reason for an effective MT density discussed above.

By using a similar procedure, an “effective defect density” can generally be obtained for any type of defect-originated scattering, when a structure contains more than one type of structural defects. An effective defect density can serve as a “figure of merit” that represents the quality of a test piece, since the effects of all structural defects on electron mobility are expressed by a single representative value.

### 6.2 Equivalent defect scattering

Here we discuss another numerical index for defect-originated electron scattering. A MT is a planar defect, while a TD is a line defect. This fundamental difference can make it difficult to directly compare the properties of these two defects. By using the results of a linear regression, however, one can assess MT-originated scattering with respect to a standardized TD-originated scattering. The

second term in the parentheses of the right side of eq. (4) shows that a given TD density  $D_{TD}$  can be converted to an equivalent MT density in terms of electron scattering by using,

$$D_{MT}^{equi} = \frac{A_{TD}}{A_{MT}} D_{TD} = 7.5 \times 10^{-6} \text{ cm} \times D_{TD} = 75 \text{ nm} \times D_{TD}. \quad (6)$$

This equation shows that the room-temperature electron scattering due to one TD in the InSb QWs examined in this study is equivalent to that due to MTs with a total length of 75 nm.<sup>13)</sup> This value is significantly larger than the length (0.23 nm) of Burgers vector of a 60°-perfect TD in InSb QWs.<sup>26)</sup> Equation (6) indicates that the electron scattering due to MTs was evaluated by using a standardized scale, which is, in this case, the electron scattering due to one TD. A similar “equivalent defect scattering” evaluation can be made for any cases where more than one type of defects causes carrier scattering, as long as  $A_{defect}$  values are available.

### 7. Conclusions

The graphical representation and the numerical interpretation of the results (defect coefficients:  $A_{defect}$ ) obtained by regression analysis for Matthiessen’s formula have been discussed for the case of electron scattering due to MTs and TDs in InSb QWs. At room temperature, 20-nm-thick InSb QWs examined in this study have a MT coefficient of  $A_{MT} = 7.9 \times 10^{-10}$  V·s/cm and a TD coefficient of  $A_{TD} = 5.9 \times 10^{-15}$  V·s. By plotting the reciprocal of total electron mobility [in the unit of  $\text{cm}^2/(\text{V}\cdot\text{s})$ ] with respect to [MT coefficient (V·s/cm)  $\times$  MT density (/cm) + TD coefficient (V·s)  $\times$  TD density (/cm<sup>2</sup>)], a 2D graphical representation that clearly shows the “goodness of fit” of the regression analysis was drawn.

In order to numerically assess the scattering efficiencies due to MTs and TDs in InSb QWs, “effective defect density” and “equivalent defect scattering”, were used. The “effective MT density” (/cm) is expressed by [MT density (/cm) +  $7.5 \times 10^{-6}$  (cm)  $\times$  TD density (/cm<sup>2</sup>)], while the “effective TD density” (/cm<sup>2</sup>) is equal to [TD density (/cm<sup>2</sup>) +  $1.3 \times 10^5$  (/cm)  $\times$  MT density (/cm)], in InSb QWs at room temperature. When the amount of electron scattering due to one TD in InSb QWs is taken as a standard, the “equivalent MT scattering” takes place when MTs have a total length of 75 nm.

### Acknowledgments

The authors would like to thank G. W. Strout and J. C. Keay for technical support. The authors also gratefully acknowledge use of the Samuel Roberts Noble Electron Microscopy Laboratory of the University of Oklahoma. This work was supported by the National Science Foundation (DMR-0520550 and DMR-0808086).

### Appendix A: Mathematical Explanation of 2D Graph

An explanation for the accurate 2D graphical expression shown in Fig. 3(a) is as follows. In order to draw a regression “line” in a 2D graph, first, the regression plane in a 3D space needs to be viewed from an edge-on direction, as demonstrated in Fig. 2(c). This condition is satisfied

when the normal (vertical) vector  $[-A_{MT}, -A_{TD}, 1]$  of the regression plane, which can be straightforwardly derived from eq. (2), is perpendicular to a viewing direction  $\mathbf{u}$ . In addition, the  $1/\mu_{total}$  axis whose directional vector can be represented by  $[0, 0, 1]$  also needs to be perpendicular to the viewing direction  $\mathbf{u}$ , in order to directly perceive the deviations between the experimental data and the regression result. From these two conditions, the viewing direction  $\mathbf{u}$  can be determined by calculating a cross product between  $[0, 0, 1]$  and  $[-A_{MT}, -A_{TD}, 1]$ , as follows:

$$\mathbf{u} = [0, 0, 1] \times [-A_{MT}, -A_{TD}, 1] = [A_{TD}, -A_{MT}, 0] \quad (A\cdot1)$$

We set the  $1/\mu_{total}$  axis as the vertical axis of the 2D graph, whose directional vector  $\mathbf{w}$  is expressed by  $\mathbf{w} = [0, 0, 1]$ . In order to draw the 2D graph, one also needs to know its horizontal axis. The horizontal axis is perpendicular to both the viewing direction  $\mathbf{u}$  and the  $1/\mu_{total}$  vertical axis. Therefore, the direction  $\mathbf{v}$  of the horizontal axis can be calculated with an equation

$$\mathbf{v} = \mathbf{w} \times \mathbf{u} = [0, 0, 1] \times [A_{TD}, -A_{MT}, 0] = [A_{MT}, A_{TD}, 0]. \quad (A\cdot2)$$

On a 2D graph that has the horizontal directional vector  $\mathbf{v}$  and the vertical directional vector  $\mathbf{w}$ , the horizontal and vertical coordinates of a given  $[D_{MT}, D_{TD}, 1/\mu_{total}]$  can be represented by

$$[D_{MT}, D_{TD}, 1/\mu_{total}] \cdot \mathbf{v} = A_{MT} D_{MT} + A_{TD} D_{TD} \quad (A\cdot3)$$

$$[D_{MT}, D_{TD}, 1/\mu_{total}] \cdot \mathbf{w} = \frac{1}{\mu_{total}}, \quad (A\cdot4)$$

respectively. Therefore, by plotting  $[(A_{MT} D_{MT} + A_{TD} D_{TD}), 1/\mu_{total}]$ , one can obtain a 2D graphical expression of eq. (2), as shown in Fig. 3(a).

### Appendix B: Angular Direction of 2D Projection

The reason for the rotation angle  $\theta = 63.4^\circ$ , which yielded a regression line in Fig. 2(c), will be discussed here. As shown in Fig. 2(b),  $15 \times 10^3/\text{cm}$  and  $4 \times 10^9/\text{cm}^2$  correspond to the full spans of the  $D_{MT}$  and  $D_{TD}$  axes in Fig. 2(c), respectively, whose actual lengths in the 3D space are the same. When only the numeric parts of these axes are taken into account, one can consider that the  $D_{MT}$  axis is effectively elongated by a factor of  $2.67 \times 10^5$  [ $= (4 \times 10^9)/(15 \times 10^3)$ ] in Fig. 2(c). If there is no such an elongation for the  $D_{MT} - D_{TD} - 1/\mu_{total}$  axes, the regression plane can be viewed as a line from the  $[A_{TD}, -A_{MT}, 0]$  direction, according to eq. (A·1). In the case of Fig. 2(c), however, the corresponding direction becomes  $[(2.67 \times 10^5) \times A_{TD}, -A_{MT}, 0]$ , since the  $A_{TD}$  value which is measured on the elongated  $D_{MT}$  axis also needs to be enlarged by a factor of  $2.67 \times 10^5$ . Therefore, the rotation angle  $\theta$  for Fig. 2(c), which is measured with respect to the  $D_{TD}$  axis, is expressed by

$$\theta = \arctan \left[ \frac{(2.67 \times 10^5) \times A_{TD}}{A_{MT}} \right]. \quad (B\cdot1)$$

By substituting the  $A_{MT}$  and  $A_{TD}$  values determined by the regression analysis,  $\theta = 63.4^\circ$  which was used for Fig. 2(c) can be obtained.

- 1) O. Madelung: *Semiconductors: Data Handbook* (Springer, Berlin, 2004) 3rd ed., p. 154.
- 2) T. D. Mishima, J. C. Keay, N. Goel, M. A. Ball, S. J. Chung, M. B. Johnson, and M. B. Santos: *J. Cryst. Growth* **251** (2003) 551.
- 3) T. D. Mishima, M. Edirisooriya, N. Goel, and M. B. Santos: *Appl. Phys. Lett.* **88** (2006) 191908.
- 4) T. D. Mishima, M. Edirisooriya, and M. B. Santos: *Appl. Phys. Lett.* **91** (2007) 062106.
- 5) S. A. Solin, D. R. Hines, A. C. H. Rowe, J. S. Tsai, Y. A. Pashkin, S. J. Chung, N. Goel, and M. B. Santos: *Appl. Phys. Lett.* **80** (2002) 4012.
- 6) V. P. Kunets, W. T. Black, Y. I. Mazur, D. Guzun, G. J. Salamo, N. Goel, T. D. Mishima, D. A. Deen, S. Q. Murphy, and M. B. Santos: *J. Appl. Phys.* **98** (2005) 014506.
- 7) S. J. Smith, G. R. Nash, C. J. Bartlett, L. Buckle, M. T. Emeny, and T. Ashley: *Appl. Phys. Lett.* **89** (2006) 111118.
- 8) X. Guan and Z. Yu: *IEEE Trans. Nanotechnol.* **6** (2007) 101.
- 9) T. G. Tenev, A. Palyi, B. I. Mirza, G. R. Nash, M. Fearn, S. J. Smith, L. Buckle, M. T. Emeny, T. Ashley, J. H. Jefferson, and C. J. Lambert: *Phys. Rev. B* **79** (2009) 085301.
- 10) V. P. Kunets, S. Easwaran, W. T. Black, D. Guzun, Y. I. Mazur, N. Goel, T. D. Mishima, M. B. Santos, and G. J. Salamo: *IEEE Trans. Electron Devices* **56** (2009) 683.
- 11) A. M. Gilbertson, P. D. Buckle, M. T. Emeny, T. Ashley, and L. F. Cohen: *Phys. Rev. B* **84** (2011) 075474.
- 12) T. D. Mishima and M. B. Santos: *J. Appl. Phys.* **109** (2011) 073707.
- 13) T. D. Mishima, M. Edirisooriya, and M. B. Santos: *J. Appl. Phys.* **110** (2011) 093705.
- 14) R. J. Egan, V. W. L. Chin, and T. L. Tansley: *J. Appl. Phys.* **75** (1994) 2473.
- 15) K. Kanisawa, H. Yamaguchi, and Y. Hirayama: *Appl. Phys. Lett.* **76** (2000) 589.
- 16) X. Weng, R. S. Goldman, D. L. Partin, and J. Heremans: *J. Appl. Phys.* **88** (2000) 6276.
- 17) X. Weng, N. G. Rudawski, P. T. Wang, R. S. Goldman, D. L. Partin, and J. Heremans: *J. Appl. Phys.* **97** (2005) 043713.
- 18) T. Sato, T. Suzuki, S. Tomiya, and S. Yamada: *Physica B* **376–377** (2006) 579.
- 19) A. N. Semenov, B. Ya. Meltser, V. A. Solovov, T. A. Komissarova, A. A. Sitnikova, D. A. Kirylenko, A. M. Nadtochiy, T. V. Popova, P. S. Kopev, and S. V. Ivanov: *Semiconductors* **45** (2011) 1327.
- 20) D. Zhao and K. J. Kuhn: *IEEE Trans. Electron Devices* **38** (1991) 2582.
- 21) T. Ohori, S. Ohkubo, K. Kasai, and J. Komeno: *J. Appl. Phys.* **75** (1994) 3681.
- 22) I. Lo, K. Y. Hsieh, S. L. Hwang, L. W. Tu, W. C. Mitchel, and A. W. Saxler: *Appl. Phys. Lett.* **74** (1999) 2167.
- 23) D. Jena, A. C. Gossard, and U. K. Mishra: *Appl. Phys. Lett.* **76** (2000) 1707.
- 24) M. Dremel, H. Priller, M. Grun, C. Klingshirn, and V. Kazukauskas: *J. Appl. Phys.* **93** (2003) 6142.
- 25) D. B. Holt and B. G. Yacobi: *Extended Defects in Semiconductors: Electronic Properties, Device Effects and Structures* (Cambridge University Press, Cambridge, U.K., 2007) pp. 412–605.
- 26) T. D. Mishima, M. Edirisooriya, and M. B. Santos: *Physica B* **376–377** (2006) 591.
- 27) T. D. Mishima and M. B. Santos: *Phys. Procedia* **3** (2010) 1373.
- 28) NIST, Physical Measurement Laboratory, Semiconductor and Dimensional Metrology Division, Hall Effect Measurements [www.nist.gov/pml/div683/hall.cfm].
- 29) The R Project for Statistical Computing [www.r-project.org].
- 30) J. M. S. Orr, A. M. Gilbertson, M. Fearn, O. W. Croad, C. J. Storey, L. Buckle, M. T. Emeny, P. D. Buckle, and T. Ashley: *Phys. Rev. B* **77** (2008) 165334.